Edge saturation fields and dynamic edge modes in ideal and nonideal magnetic film edges

R. D. McMichael and B. B. Maranville
Metallurgy Division, National Institute of Standards and Technology, Gaithersburg, Maryland 20899-8552, USA
(Received 13 January 2006; revised manuscript received 2 June 2006; published 26 July 2006)

This paper describes modeling of the micromagnetic behavior near edges of ferromagnetic thin films when uniform fields are applied in plane and perpendicular to the edge. For ideal film edges with vertical edge surfaces, the field required to saturate the magnetization perpendicular to the edge, H_{sat}, and the frequency of precession in the localized edge mode are calculated using numerical micromagnetics for a wide range of film thicknesses. Analysis of the critical state at the saturation field and the full micromagnetic results are used to develop a simple macrospin model for the edge magnetization. This model predicts both H_{sat} and edge mode precession frequency values that agree well with the micromagnetic results. Three classes of nonideal edges are also modeled: tilted edge surfaces, diluted magnetization near the edge, and surface anisotropy on the edge surface. Despite their different physical mechanisms, all three of these defects produce similar reductions in H_{sat} and similar dynamic properties of the edge magnetization.

DOI: 10.1103/PhysRevB.74.024424 PACS number(s): 75.70.Ak, 75.75.+a, 76.50.+g, 75.40.Gb

I. INTRODUCTION

In the study of nanostructured materials it is widely accepted that many properties of a material are determined by the surfaces and interfaces, and that the importance of surfaces and interfaces grows as grain sizes, particle sizes, or film thicknesses become small. Similarly, the edges of patterned magnetic thin films are expected to play an important role in the magnetic behavior of patterned elements.[1–9]

The overall properties of a thin film device may depend on the edge properties through several mechanisms. For small structures, the device behavior may depend strongly on the edge properties simply because all locations in the structure are close enough to an edge to couple to the edge magnetization via exchange and dipole-dipole interactions. In larger structures, the critical stages in magnetization reversal often include nucleation or annihilation of vortices at the edge.[4,8–13] Because these processes occur at the film edge, the edge properties play an important role in the reversal.

Despite the demonstrated importance of edge properties to device behavior, relatively little work has been done to develop methods for characterizing the magnetic properties of thin film edges. One recently explored path toward magnetic edge characterization involves measurements of the magnetization dynamics in transversely magnetized, long, straight stripes. In this configuration, inhomogeneous magnetostatic fields localize magnetization precession near the edge in a trapped spinwave edge mode.[14–21]

Figure 1 shows typical static and dynamic properties of a magnetic stripe in a transverse field as calculated by numerical micromagnetics.[21–23] The quasistatic behavior is best described in terms of three field ranges. At the lowest fields, M_x is small and the magnetization lies mostly along the stripe axis in the y direction. Above an indistinct bulk saturation field indicated by a dashed line in Fig. 1, the center of the stripe is nearly saturated perpendicular to the stripe axis, but a significant component of the magnetization remains in the y direction near the stripe edges.[24] At fields above the indicated edge saturation field, H_{sat}, the magnetization at the edge aligns very nearly parallel to the applied field.

The behavior of the magnetization curves is also reflected in the resonance frequencies of the magnetic normal modes in the stripes. At the lowest fields where the magnetization lies nearly parallel to the stripe axis, the normal modes in similar systems have been described as standing spin waves propagating perpendicular to the stripe axis with the dynamic magnetostatic fields creating effective pinning conditions at edges.[15,25–27] Near the indistinct bulk saturation field, the lowest resonance frequency goes through a minimum, and at slightly higher fields the edge mode (lowest frequency) becomes distinct from the bulk modes.[14–17,20,24]

For this paper, the primary interest is in the edge mode for fields near and above H_{sat}. The edge saturation field H_{sat}, where M_y and the edge mode frequency both go to zero, is an important quantity that characterizes the magnetic properties of the edge. At H_{sat}, the edge magnetization is neutrally stable and the "softness" of the edge magnetization in this state is reflected in the zero edge mode frequency. For fields greater than H_{sat}, the equilibrium magnetization is aligned in

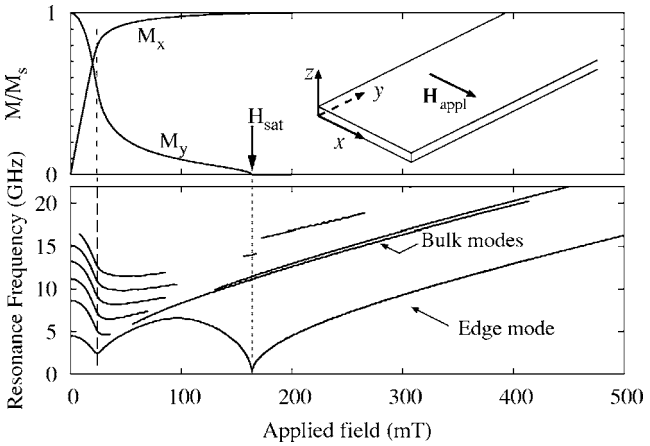

FIG. 1. Static magnetization curves (top) and resonance frequencies (bottom) for a permalloy stripe, 480 nm wide and 12 nm thick, with "ideal" edges. The center of the stripe is mostly saturated at 24 mT and the indicated critical field H_{sat} for edge saturation is 164 mT.

the x direction. However, there is a dipolar field equal to $-M_s/2$ at the edge surface. For fields between H_{sat} and $M_s/2$ then, there is a region of negative field near the edge where the magnetization is stabilized in the positive direction by exchange interactions.

While H_{sat} is easily obtained from the computational experiments, laboratory experiments may encounter difficulties in determining H_{sat} owing to alignment tolerances. Our previous calculations have shown that for fields applied as little as 1° away from the x direction, H_{sat} becomes indistinct in the magnetization curves and the edge mode frequency minimum becomes rounded and shifted to higher field.[23]

The localized nature of the precession in an edge mode makes the mode sensitive to edge conditions. In transversely saturated stripes, significant differences have been found between experimentally measured edge mode frequencies and the edge mode frequencies predicted for ideal edges.[23,24] Further evidence for the sensitivity of edge modes to edge conditions has been revealed by time resolved Kerr microscopy where differences have been observed between the edge mode frequencies on opposite edges of the same stripe.[16,20] Tilted edge surfaces have been proposed as a possible mechanism to explain differences between measured edges and modeled ideal edges.[23,24] However, it will be shown below that edge surface tilting is only one of several possible microstructural conditions that affect the magnetic edge behavior in similar ways.

This paper describes computational experiments and modeling designed to determine the magnetic behavior of thin film edges with different microstructural properties. In Sec. II, we describe some of the properties of "ideal" edges with smooth, vertical side walls, uniform intrinsic properties, and no surface anisotropy. In Sec. III, the effects of three possible types of edge "defect" on the edge saturation field are separately investigated by varying (1) the geometric profile of the edge surface, (2) the dilution of both the spontaneous magnetization M_s and exchange stiffness A near the edge, and (3) the presence of a surface anisotropy on the edge surface.

II. IDEAL EDGES

This section describes some of the properties of ideal edges as a function of film thickness. We begin by considering the fields near the edge of a half-infinite film of thickness t bounded by $x>0$ and $0<z<t$. If the magnetization is assumed to be independent of y, the field inside the film at a position $\mathbf{r}\equiv(x,z)$ is given by

$$\mathbf{H}(\mathbf{r}) = \mathbf{H}_{\text{appl}} + l_{\text{ex}}^2\nabla^2\mathbf{M}(\mathbf{r}) + \int_0^\infty dx' \int_0^t dz' \frac{2(\widehat{\mathbf{r}'-\mathbf{r}})(\widehat{\mathbf{r}'-\mathbf{r}})-\mathbf{1}}{2\pi|\mathbf{r}'-\mathbf{r}|^2}\cdot\mathbf{M}(\mathbf{r}'), \quad (1)$$

including a uniform applied field, the exchange field, and the magnetostatic field, respectively. The exchange length, l_{ex} depends on the exchange stiffness A and the saturation magnetization M_s: $l_{ex}^2=2A/(\mu_0 M_s^2)$. The hat notation indicates a unit vector, $\hat{\mathbf{r}}\equiv\mathbf{r}/|\mathbf{r}|$.

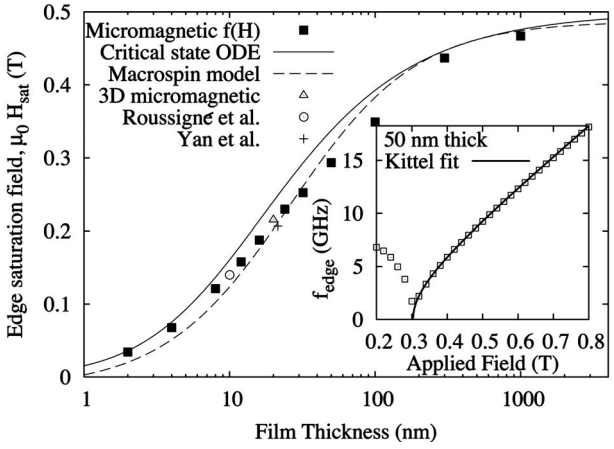

FIG. 2. Edge saturation fields obtained from micromagnetic calculations (Sec. II A), including a point from a 3D calculation and data from Refs. 21 and 22. Curves are from a model based on analysis of the critical state (Sec. II C) and a macrospin model (Sec. II B). Inset, field dependence of edge mode frequencies. The solid line is a fit described in the text.

The dynamic behavior of the normalized magnetization $\hat{\mathbf{m}}=\mathbf{M}/M_s$ is given by the Landau-Lifshitz-Gilbert equations of motion,[28,29]

$$\frac{d\hat{\mathbf{m}}}{dt} = -\omega_M[\hat{\mathbf{m}}\times\mathbf{h}] + \alpha\hat{\mathbf{m}}\times\frac{d\hat{\mathbf{m}}}{dt}, \quad (2)$$

where $\omega_M\equiv\gamma M_s$ with $\gamma=2.211\times10^5$ m/(As), $\mathbf{h}\equiv\mathbf{H}/M_s$ is the normalized effective field, and α is the Gilbert damping parameter.

Making the transformation to unitless coordinates $\boldsymbol{\rho}=(\xi,\zeta)\equiv(x,z)/l_{ex}$ and $\tau=t/l_{ex}$, the normalized field is given by

$$\mathbf{h}(\boldsymbol{\rho}) = \mathbf{H}_{\text{appl}}/M_s + \nabla_\rho^2\hat{\mathbf{m}}(\boldsymbol{\rho}) + \int_0^\infty d\xi' \int_0^{t/l_{ex}} d\zeta' \frac{2(\widehat{\boldsymbol{\rho}'-\boldsymbol{\rho}})(\widehat{\boldsymbol{\rho}'-\boldsymbol{\rho}})-\mathbf{1}}{2\pi|\boldsymbol{\rho}'-\boldsymbol{\rho}|^2}\cdot\hat{\mathbf{m}}(\boldsymbol{\rho}'). \quad (3)$$

For this paper, the magnetic film edge properties are explicitly calculated for material properties corresponding to permalloy films. However, from (3) it is clear that the film thickness enters the equations of motion only in the ratio $\tau=t/l_{ex}$, and that the applied field enters the equations of motion only in the ratio $\mathbf{H}_{appl}/M_s$. These ratios provide a method for scaling the permalloy results to obtain ideal edge properties for films of other magnetic materials.

The following sections describe three models that provide estimates of H_{sat} for ideal edges on films of varying thicknesses. The results are collected in Fig. 2.

A. Numerical micromagnetics

Computational experiments were performed using the OOMMF micromagnetic code[30] to model isolated stripes with material parameters approximating permalloy ($Ni_{80}Fe_{20}$); spontaneous magnetization $M_s=800$ kA/m, ex-

change stiffness $A=13$ pJ/m and damping parameter $\alpha=0.01$. With these parameters, the exchange length for this material is $l_{ex}=(2A/\mu_0 M_s^2)^{1/2}\approx 5.7$ nm. The boundary condition at the top, bottom, and edge surfaces is assumed to be free, i.e., there are no surface torques and consequently, for surface normal vector $\hat{\mathbf{n}}$, $d\mathbf{M}/d\hat{\mathbf{n}}=0$.

We performed a number of calculations for stripes of different thicknesses, keeping the width to thickness aspect ratio of the stripe between values of 15 and 240. The stripe width was kept larger than 300 nm to allow for the fact that the effects of the edge extend into the bulk. A quasi-two-dimensional approach was implemented by making the cells very long in the y direction [along the stripe axis, see Fig. 1(a)]. In the x and z directions a variety of cell sizes were used. For films thinner than 32 nm thick, 1 nm or 2 nm cells were used, while for films thicker than 32 nm the thickness was divided into 16 cells. Although these cells are larger than the exchange length, they are small enough to yield smooth static magnetization and mode profiles without large angles between neighboring spins.

The validity of the two-dimensional (2D) approach was verified by a much more computationally demanding three-dimensional (3D) calculation of edge saturation in a 250 nm wide, 4 μm long, 20 nm thick, permalloy rectangle using 4 nm$\times$4 nm$\times$5 nm cells. Relative to the infinite stripes of the 2D model, the edge saturation transition was broadened somewhat by the broken symmetry near the ends.

We used a field-pulse process to calculate the dynamic properties of the stripes.[31–33] First, we used an energy minimization scheme to allow the magnetization to come to equilibrium in the applied field. The magnetization dynamics were then excited by a short, spatially uniform field pulse. The pulse field rotated the magnetization approximately 1° away from equilibrium with 1.0 T applied for 100 fs in the z direction. The short duration field pulse is equivalent to a broadband excitation that is essentially flat to frequencies much greater than 100 GHz.

Following the field pulse, the magnetization motion was calculated using the Landau-Lifshitz-Gilbert equations of motion (2). The resulting time series $M_z(\mathbf{r}_i,t)$ for each micromagnetic cell i, and the spatial average of the magnetization $\langle M_z(t)\rangle$ were recorded. These time series were Fourier transformed to obtain the frequency response of the stripe. The Fourier transforms are proportional to the susceptibility functions $\chi(\mathbf{r}_i,f)$ and $\langle\chi(f)\rangle$ for the local and spatially averaged magnetization, respectively. Peaks in the imaginary part of $\langle\chi(f)\rangle$ correspond to the peaks one would observe in a broadband ferromagnetic resonance experiment.

For a resonance in $\langle\chi(f)\rangle$ occurring at a frequency f_j^{res}, the spatial profile of the corresponding normal mode (or superposition of modes) is obtained from $\chi(\mathbf{r}_i,f_j^{\mathrm{res}})$.[32,33] These profiles enable one to identify resonances as bulk or edge modes, and they show the degree of localization of edge modes.

For film thicknesses less than roughly 30 nm, $\langle\chi(f)\rangle$ exhibits only a few strong resonances, including a single edge mode and one or two bulk modes as shown in Fig. 1. Typically, a number of weaker resonances are also detected at higher frequencies. In films thicker than 30 nm, there are multiple edge modes and multiple bulk modes. In these cases we report only the lowest edge mode frequency. Multiple edge modes have previously been observed experimentally.[17]

The field near one edge of a transversely magnetized stripe includes a component H^{opp} from the magnetostatic charges near the opposite edge. For a stripe with film thickness t and stripe width w, the field due to these charges is $H^{\mathrm{opp}}\approx -M_s t/(2\pi w)$ for $t\ll w$. Field values reported below and in Fig. 2 have been corrected by an amount equal to H^{opp} in order to represent fields more characteristic of a single edge than of a particular finite width stripe.

For fields greater than the edge saturation field, we fit the computed edge mode frequencies to a Kittel frequency of the form

$$f(H_{\mathrm{appl}})=\frac{\mu_0\gamma}{2\pi}[(H_{\mathrm{appl}}+H_1)(H_{\mathrm{appl}}+H_2)]^{1/2}. \tag{4}$$

In Sec. II B, the physical significance of H_1 and H_2 is described in terms of magnetostatic and exchange fields, but here they may be regarded simply as fitting parameters. An example fit is shown in the inset of Fig. 2. We arbitrarily assign $H_1<H_2$. The saturation field is identified as the field where the precession field drops to zero and the magnetization becomes neutrally stable, or $H_{\mathrm{sat}}=-H_1$. For thinner films, a good fit can be made for fields well above H_{sat}. For the thickest films, good fits were only obtained when the fitted data were restricted to fields within a few tens of mT of H_{sat}. The fit values for H_{sat} are plotted as points in Fig. 2.

We suspect that part of the problem in fitting the thick film edge resonance frequencies lies in the fact that the equilibrium state is field dependent in the thicker films. For films thicker than a few exchange lengths, the equilibrium state includes a spreading of the magnetization direction near the edge surface, with a significant z component of the magnetization on the top corner and an oppositely directed z component on the bottom corner.[18] The degree of spreading in the ground state depends on the applied field, vanishing in the limit of infinite applied field. This effect is smaller in the thinner films where exchange interactions force magnetization near the top and bottom surfaces to lie parallel.

B. Macrospin model

This section describes a simple macrospin model of the edge magnetization. Equation (4) was used above to fit edge mode frequencies, but it is also identical to the expression one would use to describe the resonance frequency of the magnetization in an ellipsoid-shaped sample. The macrospin model is based on determining the effective ellipsoid with the behavior that most closely matches the micromagnetic results.

A rigorous treatment of the edge dynamics using the field given in (1) would require solution of an integro-differential equation.[16,17,19,26,27] To obtain a simpler analytical result, we assume that for applied fields greater than the edge saturation field, the magnetization lies primarily in the x direction with small deviations $m_y\equiv M_y/M_s$ and $m_z\equiv M_z/M_s$. The effective field includes the applied field H_{appl}, exchange fields H_{ex} arising from exchange coupling between the edge region and

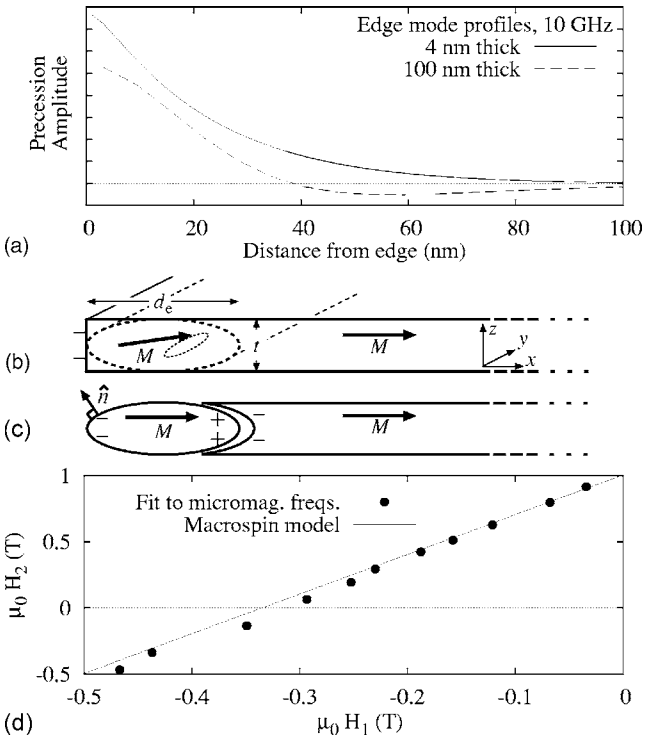

FIG. 3. (a) 10 GHz edge mode precession profiles determined by numerical micromagnetics for 4 nm and 100 nm films. (b) Geometry of the macrospin model showing precession confined to a region bounded by an elliptical cylinder near the edge. (c) In the elliptical region the magnetostatic field differs from the field in a free elliptical cylinder because of the attached sheet film. (d) Values of H_2 from fits of the micromagnetic edge mode frequencies (squares) compared with the prediction of the macrospin model.

the bulk of the film and magnetostatic fields given by effective demagnetization factors N_x^{eff}, N_y^{eff}, and N_z^{eff},

$$H_x = H_{\text{appl}} - N_x^{\text{eff}} M_s, \tag{5}$$

$$H_y = -H_{\text{ex}} m_y - N_y^{\text{eff}} M_s m_y, \tag{6}$$

$$H_z = -H_{\text{ex}} m_z - N_z^{\text{eff}} M_s m_z. \tag{7}$$

Using this expression for the field in the precession region, the precession frequency obtained from (2) has the form of (4) with

$$H_1 = H_{\text{ex}} + (N_y^{\text{eff}} - N_x^{\text{eff}}) M_s, \tag{8}$$

$$H_2 = H_{\text{ex}} + (N_z^{\text{eff}} - N_x^{\text{eff}}) M_s. \tag{9}$$

The exchange field and the effective demagnetization factors are expected to depend on the spatial profile of the edge mode, characterized by a localization length scale d_e that describes the depth that the edge mode extends into the bulk of the film. Figure 3(a) shows that edge mode profiles are relatively insensitive to thickness at 10 GHz. Despite the fact that the thicknesses differ by well over an order of magnitude, the edge mode precession extends approximately the same distance into the film. The very weak dependence of the edge mode depth on the film thickness is also confirmed in Sec. II C, below. Because the edge mode depth d_e is only weakly dependent on film thickness, we make the approximation that d_e is independent of thickness.

Next, approximate expressions for the effective demagnetization factors are developed, assuming that the precession is confined to a region that is an elliptical cylinder lying along the film edge with primary axes equal to the thickness, t and the edge mode depth d_e. See Fig. 3(b).

As shown in Fig. 3(c), for a free-standing elliptical cylinder magnetized in the x direction, positive and negative magnetostatic surface charges on opposite "sides" of the ellipse give rise to a demagnetization field $H_x^{\text{demag}} = -N_x M_s$ with $N_x = t/(t+d_e)$. However, the negative charges on the concave surface of the film edge exactly cancel the positive charges on the right half of the ellipse in Fig. 3(c). Since only half of the charges remain, we take one-half of the demagnetization factor for the free standing cylinder as an approximate demagnetization factor for the cylinder embedded in the film edge;

$$N_x^{\text{eff}} = \frac{1}{2}\frac{t}{t+d_e}. \tag{10}$$

The magnetization in the bulk of the film does not contribute to fields in the y or z directions. The remaining demagnetization factors are therefore,

$$N_y^{\text{eff}} = 0, \tag{11}$$

$$N_z^{\text{eff}} = \frac{d_e}{t+d_e}. \tag{12}$$

With these effective demagnetization factors, the macrospin model of the edge saturation field is

$$H_{\text{sat}} = -H_1 = -H_{\text{ex}} + \frac{M_s}{2}\frac{t}{t+d_e}. \tag{13}$$

Values for H_{ex} and d_e were determined by fitting (13) to the micromagnetic saturation fields (i.e., the black squares in Fig. 2). The fits yield essentially zero for $H_{\text{ex}} = (-1.0 \pm 11)$ mT and $d_e = (26 \pm 3)$ nm or $d_e = (4.6 \pm 0.6)\, l_{\text{ex}}$. The fit is shown as a solid line in Fig. 2(a). Note the excellent agreement between the approximate macrospin model and the full micromagnetic result over 3 orders of magnitude variation in stripe thickness.

The small value of H_{ex} obtained from the fit to the micromagnetic H_{sat} data is somewhat surprising. Given an edge mode depth of $d_e \approx 26$ nm that is consistent with the edge mode profiles shown in Fig. 3(a) and Fig. 4 below, the corresponding direct estimate is $H_{\text{ex}} \approx 2A/(M_s d_e^2) = 48$ mT.

The macrospin model also provides an estimate of the edge mode frequency for an ideal edge. Using the approximate expressions (12) and (10) above for the demagnetization factors N_z^{eff} and N_x^{eff}, one can derive a relationship between H_1 and H_2,

$$H_2 = M_s + 3H_1 - 2H_{\text{ex}}. \tag{14}$$

This relation is plotted as a solid line in Fig. 3(d) using $H_{\text{ex}} = 0$ and $\mu_0 M_s = 1.0$ T. Pairs of H_1 and H_2 values obtained from micromagnetic calculations are also plotted for com-

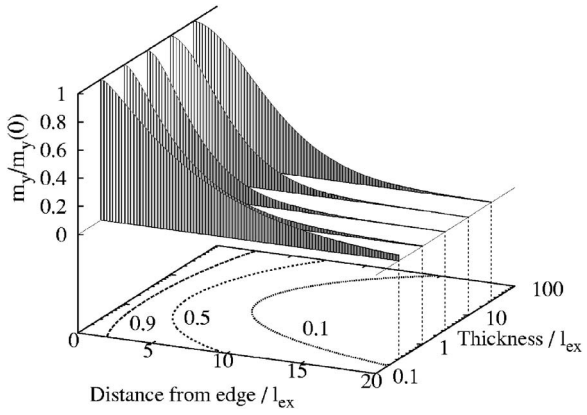

FIG. 4. Zero frequency edge mode profiles at $H_{appl}=H_{sat}$ obtained by solution of (16). A few mode profiles are shown above and selected contours for a large set of solutions are shown on the base. The profile of the magnetization tilting in the zero frequency edge mode does not depend sensitively on the film thickness.

parison. Note that the micromagnetic data points fall very close to the macrospin model line, consistent with $H_{ex}\approx 0$. Using values of H_1 and H_2 from (13) and (14), respectively, an estimate of the edge mode frequency is given by (4).

C. Critical state analysis

This section contains an analysis of the behavior of the magnetization at the saturation field. The results of this analysis include a third estimate of the edge saturation field and confirmation of the weak dependence of the edge mode depth on the film thickness. The stripe is assumed to be nearly uniformly magnetized in the x direction, with a small deviation $m_y(x)=M_y(x)/M_s$. The magnetostatic field is the field due to the uniform sheet of magnetic charges on the edge surface. The field inside the film is approximated by considering only the field along the center plane of the stripe at $z=t/2$.

$$H_d(x) = -\frac{1}{\pi} M_s \arctan\left(\frac{t}{2x}\right), \tag{15}$$

where t is the thickness, x is the distance from the edge, and M_s is the saturation magnetization. As in Sec. II, the distances in the equation are normalized by the exchange length l_{ex} so that $\xi=x/l_{ex}$ and $\tau=t/l_{ex}$. In equilibrium, the net torque on each moment is zero,

$$\frac{d^2 m_y}{d\xi^2} - \left[\frac{H_{appl}}{M_s} - \frac{1}{\pi}\arctan\left(\frac{\tau}{2\xi}\right)\right] m_y = 0. \tag{16}$$

The first term in Eq. (16) is the torque due to exchange interactions and the second term is the torque on the magnetization due to the local field in square brackets.

The boundary conditions are determined by considering the effect of a surface torque applied at $\xi=0$. For applied fields greater than H_{sat}, a small static torque applied at the edge surface will create a small, static tilting of the magnetization. In this state, the external torque applied to the surface magnetization is balanced by an exchange torque arising from the magnetization bending near the edge surface, $dm_y/d\xi\neq 0$.[34] For an applied field equal to the saturation field, m_y will be neutrally stable so that a finite m_y can exist when there is zero torque applied at the edge surface, and therefore no magnetization bending at the interface. Therefore, when $H_{appl}=H_{sat}$, the following boundary conditions apply:

$$\left(\frac{dm_y}{d\xi}\right)_{\xi=0} = 0, \tag{17}$$

$$(m_y)_{\xi\to\infty} = 0. \tag{18}$$

The second boundary condition ensures that the edge effects do not extend deep into the film. We find values of H_{sat} that satisfy these boundary conditions by integrating (16) from $\xi=0$ to a large value of ξ ($x=300l_{ex}$ in this case) and we use a Newton's method solver to find values of H_{appl} that give $m_y=0$ at the end of the integration.

For each film thickness, we obtain a value for H_{sat} and a solution for m_y, which is a profile of the edge mode at zero frequency. The saturation field calculated in this way is plotted vs the film thickness in Fig. 2.

Profiles of the zero frequency edge mode at $H_{appl}=H_{sat}$ are shown in Fig. 4. Note that the static magnetization tilting profile is relatively insensitive to the film thickness. The depth of the mode profile as determined by the $m_y=0.5$ contour varies by just over a factor of 2 as the thickness spans three orders of magnitude.

III. NONIDEAL EDGES

This section explores the behavior of the edge saturation field when the edges are made nonideal. The discussion is limited to edges that are uniform along the length of the edge. Edge roughness is certainly an important edge characteristic,[1–5,7–9] but it is not addressed explicitly here. In the following sections micromagnetic models of three types of nonideal edges are described. The behavior of the edge saturation field H_{sat} is compared for the three types of edges on 12 nm thick films. This thickness corresponds to an ideal edge saturation field of 164 mT that lies roughly midway between the maximum and minimum values plotted in Fig. 2(a).

A. Edge geometry

One way that real edges may differ from the ideal is in the geometric profile of the edge surface.[23,24] Faceting may occur during chemical or plasma etching processes, or edges with tapered thickness may be formed by deposition through a shadow mask. As an initial model of these geometric effects, we introduce tilting of the edge surface by an angle ψ. See the inset of Fig. 5(a). Values of H_{sat} for a range of tilt angles ψ are given in Fig. 5(a), showing that edge surface tilting tends to reduce H_{sat}.

The x component of the internal field for a 45° edge profile is shown in Fig. 6(a). Different edge defects will create different distributions of magnetostatic charge. To facilitate comparison between different types of defects, the x axis in

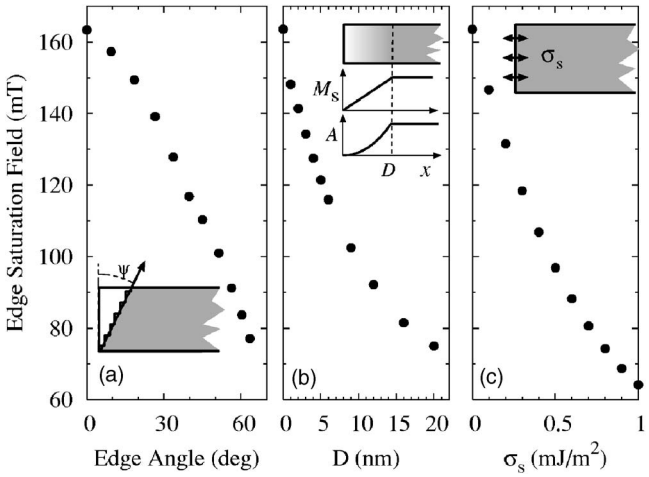

FIG. 5. Edge saturation field for 12 nm thick permalloy stripes with various edge properties. (a) H_{sat} as a function of the edge surface angle. (b) H_{sat} as a function of the width of a diluted region at the edge. The magnetization M_s drops linearly to zero over the distance D, and the exchange stiffness is set proportional to M_s^2. (c) H_{sat} as a function of surface anisotropy energy on the edge surface.

Fig. 6 is the horizontal distance from the magnetostatic charge center.

For a 12 nm thick film, saturated in the x direction, the magnetostatic edge charges are distributed uniformly over the edge surface extending from $x=0$ nm, $z=0$ nm to $x=12$ nm, $z=12$ nm. The charge center is therefore located at $x=6$ nm. The field values shown are taken from the midplane of the stripe, $z=t/2$ for $x>12$ nm and $z=x/2$ for $x<12$ nm. The internal field for the tilted edge begins to differ noticeably from ideal edge case near 6 nm away from the charge center, approximately coincident with the location of the top end of the charged edge surface.

The large increases in the internal field that are observed to the left of the charge center occur because some charges are located further from the edge than the observation point.

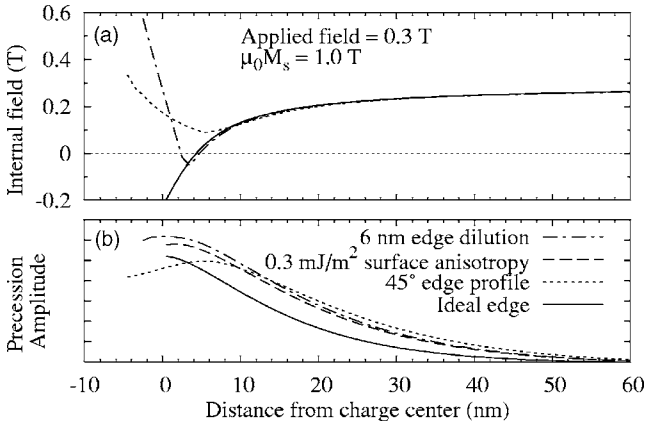

FIG. 6. (a) Profiles of the x component of the internal field at the midplane for 12 nm thick stripes of permalloy with different edge properties. The internal field for the edge with surface anisotropy is identical to the field for an ideal edge. (b) Thickness-averaged edge mode precession amplitude profiles at $H_{appl}=0.3$ T for various edge conditions.

Right at the knife edge of the taper, where the edge surface meets the bottom surface in Fig. 5(a), the field due to the surface charges actually adds to the applied field, for a net field greater than the applied field of 0.3 T. The net effect is that tilting of the edge surface reduces the saturation field by reducing the magnitude of the magnetostatic field in the neighborhood of the edge.

B. Edge dilution

In films patterned by focused ion beam (FIB), the edges will be doped with Ga atoms, and this is known to "poison" the magnetization near the edge. To model this phenomenon, a vertical edge surface is assumed and the saturation magnetization is decreased linearly over a distance D from its bulk value to zero at the physical edge of the sample. Simultaneously, we modify the exchange stiffness A in this region to be proportional to $M(x)^2$. See the inset of Fig. 5(b). This choice is motivated by the spin-spin nature of the exchange interaction, and that the exchange energy might therefore be expected to depend quadratically on the magnitude of the spins. Setting A proportional to $M(x)^2$ has the interesting additional feature that the exchange length remains constant through the diluted region.

Edge dilution distributes the magnetostatic charge evenly over a volume between $x=0$ and $x=D$, so the charge center is located at $x=D/2$. Similarly to the preceding tilted edge example, spreading of the magnetostatic charges into the bulk creates a region at the geometrical edge where the demagnetization field actually adds to the applied field. The net effect is that magnetization dilution at the edges will reduce H_{sat}, as shown in Fig. 5(b).

C. Surface anisotropy

The presence of surface anisotropy on the edge surfaces has been recognized as a possibly important parameter for the switching behavior of small magnetic elements.[6] The surface anisotropy energy density is typically written in the form $-\sigma_s m_x^2$. Typical values for surface anisotropy measured in permalloy films are positive and are in the neighborhood of $\sigma_s \approx 0.1$ mJ/m^2.[6] Because the surface anisotropy energy is minimum when the magnetization points normal to the surface, the surface anisotropy will favor magnetization normal to the edge surface and it will therefore reduce H_{sat}.

For the micromagnetic calculations with cell size Δ, the surface anisotropy was implemented by including a uniaxial anisotropy energy density $K_1=\sigma_s/\Delta_x$ only in those cells having boundaries on the edge surface. The effect of surface anisotropy on H_{sat} is shown in Fig. 5(c).

D. Edge diagnostics

The previous three sections demonstrate that there are a variety of edge conditions that may cause real edges to behave differently from the ideal edges described in Sec. II. The three specific defects shown here all tend to decrease H_{sat}, but other types of edge conditions, including negative

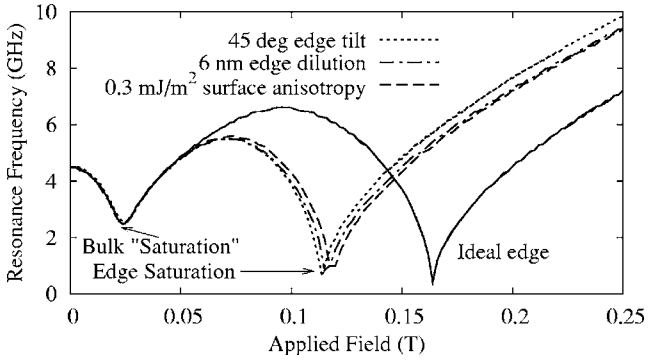

FIG. 7. Mode frequencies for a stripe with ideal edges and for three stripes with different edge properties adjusted to produce approximately the same saturation field.

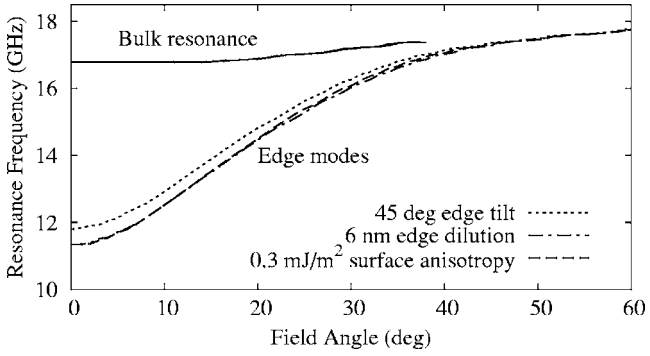

FIG. 8. Mode frequencies as a function of the direction of the in-plane applied field. Results are plotted for three stripes with different edge properties adjusted to produce approximately the same saturation field. The applied field magnitude is 0.3 T.

σ_s and/or thickening of the film near the edge may be expected to increase H_{sat}.

Given that there are a number of conditions that lead to nonideal edge behavior, it would be desirable to develop magnetic techniques to identify the conditions that are responsible for nonideal edge behavior in a particular sample. In Ref. 22 it was recognized that the edge tilting breaks the symmetry through the $z=t/2$ plane, causing splitting of the edge mode resonances as the applied field and equilibrium magnetization are rotated out of plane. In contrast, edge dilution and surface anisotropy do not break the z symmetry.

To explore other possible differences in behavior between edges with different types of defects, we model three edges with different edge properties but roughly the same value of H_{sat}. We have chosen three edges in 12 nm thick permalloy with (1) 45° edge surface tilting, (2) magnetization dilution over 6 nm, and (3) 0.3 mJ/m^2 surface anisotropy. All three of these conditions produce a value of $H_{\text{sat}} \approx 0.11$ T.

The internal field profiles (discussed above) and the profiles of the edge precession amplitude for these three edges are plotted in Fig. 6. The precession amplitude profiles are different enough to be distinguishable, but measurement on the time scales and length scales involved would be a daunting technical challenge.

Instead, we look for differences in the edge mode frequency, which can be detected by ferromagnetic resonance and Brillouin light scattering. Figure 7 plots the lowest resonance frequency as a function of applied field. The field direction is in the sample plane, perpendicular to the long axis of the stripe. In each curve, there are two minima; the rounded, low-field minimum corresponding to the near saturation of the center of the stripe and the sharp minimum corresponding to the saturation of the edge. It is clear from this figure that although the saturation field has been modified by three different mechanisms, the applied field dependences of the edge mode frequencies are nearly identical.

Figure 8 shows the edge mode frequencies for stripes with these three different edges as a function of applied field direction as the applied field of 0.3 T is rotated away from the x direction in the x-y plane. The angular dependence of the edge mode frequencies is nearly identical for the three different edge conditions. The lines for the 6 nm wide dilution region and for the 0.3 mJ/m^2 surface anisotropy are nearly superimposed in this plot.

From the standpoint of potential diagnostic measurements, it appears that for a given edge saturation field, neither the field dependence nor the in-plane angular dependence of the edge mode frequency will differentiate between possible mechanisms for deviations from ideal edge behavior. While the presence of top-bottom asymmetry can be revealed by out-of-plane angular dependence of the edge mode frequency,[23] the effects of surface anisotropy and edge dilution are effectively identical.

IV. DISCUSSION

The primary results of this paper are threefold. First, the edge saturation field is identified as a measurable quantity that characterizes an edge. Second, three models are developed to describe the thickness dependence of the edge saturation field and the edge mode frequency in ideal edges. Numerical micromagnetics and analysis of the equilibrium condition at the saturation field both reveal that the edge behavior extends into the film on the order of five exchange lengths, a distance that is only weakly dependent on the film thickness. This behavior is incorporated into a simple macrospin model of an ideal edge that is in good agreement with the full micromagnetic results. Third, three classes of nonideal edges are modeled, different nonideal edge conditions produce similar effects on the edge saturation field and on the edge mode dynamics.

Despite the fact that coercivity depends on many different microstructural features and mechanisms, it is a useful quantity for characterizing magnetic materials. Analogously, we regard the edge saturation field as a useful quantity for characterizing magnetic thin film edges.

[1] M. Herrmann, S. McVitie, and J. H. Chapman, J. Appl. Phys. **87**, 2994 (2000).
[2] R. P. Cowburn, J. Phys. D **33**, R1 (2000).
[3] J. G. Deak and R. H. Koch, J. Magn. Magn. Mater. **213**, 25 (2000).
[4] K. J. Kirk, M. R. Scheinfein, J. N. Chapman, S. McVitie, M. F. Gillies, B. R. Ward, and J. G. Tennant, J. Phys. D **34**, 160 (2001).
[5] M. T. Bryan, D. Atkinson, and R. P. Cowburn, Appl. Phys. Lett. **85**, 3510 (2004).
[6] J. O. Rantschler, P. J. Chen, A. S. Arrott, R. D. McMichael, W. F. Egelhoff, Jr., and B. B. Maranville, J. Appl. Phys. **97**, 10J113 (2005).
[7] M. R. Scheinfein (private communication).
[8] J. W. Lau, M. Beleggia, M. A. Schofield, G. F. Neumark, and Y. Zhu, J. Appl. Phys. **97**, 10E702 (2005).
[9] J. Gadbois and J.-G. Zhu, IEEE Trans. Magn. **31**, 3802 (1995).
[10] J. Shi, S. Tehrani, and M. R. Scheinfein, Appl. Phys. Lett. **76**, 2588 (2000).
[11] K. Y. Guslienko, V. Novosad, Y. Otani, H. Shima, and K. Fukamichi, Phys. Rev. B **65**, 024414 (2002).
[12] W. Scholz, K. Y. Guslienko, V. Novosad, D. Suess, T. Schrefl, R. W. Chantrell, and J. Fidler, J. Magn. Magn. Mater. **266**, 155 (2003).
[13] J. G. Deak, IEEE Trans. Magn. **39**, 2510 (2003).
[14] M. Bailleul, D. Olligs, C. Fermon, and S. O. Demokritov, Europhys. Lett. **56**, 741 (2001).
[15] J. Jorzick, S. O. Demokritov, B. Hillebrands, M. Bailleul, C. Fermon, K. Y. Guslienko, A. N. Slavin, D. V. Berkov, and N. L. Gorn, Phys. Rev. Lett. **88**, 047204 (2002).
[16] J. P. Park, P. Eames, D. M. Engebretson, J. Berezovsky, and P. A. Crowell, Phys. Rev. Lett. **89**, 277201 (2002).
[17] C. Bayer, S. O. Demokritov, B. Hillebrands, and A. N. Slavin, Appl. Phys. Lett. **82**, 607 (2003).
[18] Y. Roussigné, S.-M. Chérif, and P. Moch, J. Magn. Magn. Mater. **263**, 289 (2003).
[19] G. Gubbiotti, M. Conti, G. Carlotti, P. Cendeloro, E. Di Fabrizio, K. Y. Guslienko, A. Andre, C. Bayer, and A. N. Slavin, J. Phys.: Condens. Matter **16**, 7709 (2004).
[20] C. Bayer, J. P. Park, H. Wang, M. Yan, C. E. Campbell, and P. A. Crowell, Phys. Rev. B **69**, 134401 (2004).
[21] Y. Roussigné, S.-M. Chérif, and P. Moch, J. Magn. Magn. Mater. **268**, 89 (2004).
[22] M. Yan, H. Wang, P. A. Crowell, and C. E. Campbell, Condens. Matter Theor. **20**, 251 (2005).
[23] B. B. Maranville, R. D. McMichael, S. A. Kim, W. L. Johnson, C. A. Ross, and J. Y. Cheng, J. Appl. Phys. **99**, 08C703 (2006).
[24] M. Bailleul, D. Olligs, and C. Fermon, Phys. Rev. Lett. **91**, 137204 (2003).
[25] P. H. Bryant, J. F. Smyth, S. Schultz, and D. R. Fredkin, Phys. Rev. B **47**, 11255 (1993).
[26] K. Y. Guslienko, S. O. Demokritov, B. Hillebrands, and A. N. Slavin, Phys. Rev. B **66**, 132402 (2002).
[27] K. Y. Guslienko and A. N. Slavin, Phys. Rev. B **72**, 014463 (2005).
[28] L. D. Landau and E. M. Lifshitz, Phys. Z. Sowjetunion **8**, 153 (1935).
[29] T. L. Gilbert, IEEE Trans. Magn. **40**, 3443 (2004).
[30] M. J. Donahue and D. G. Porter, *Interagency Report NISTIR 6376* (National Institute of Standards and Technology, Gaithersburg, MD, 1999).
[31] O. Gérardin, H. Le Gall, M. J. Donahue, and N. Vukadiniovic, J. Appl. Phys. **89**, 7012 (2001).
[32] R. D. McMichael and M. D. Stiles, J. Appl. Phys. **97**, 10J901 (2005).
[33] M. Grimsditch, G. K. Leaf, H. G. Kaper, D. A. Karpeev, and R. E. Camley, Phys. Rev. B **69**, 174428 (2004).
[34] G. T. Rado and J. R. Weertman, J. Phys. Chem. Solids **11**, 315 (1959).